

Quantum mechanical calculation of Rydberg-Rydberg autoionization rates

Martin Kiffner^{1,2}, Davide Ceresoli³, Wenhui Li^{1,4}, and Dieter Jaksch^{2,1}

Centre for Quantum Technologies, National University of Singapore, 3 Science Drive 2, Singapore 117543¹

Clarendon Laboratory, University of Oxford, Parks Road, Oxford OX1 3PU, United Kingdom²

Istituto di Scienze e Tecnologie Molecolari CNR, via Golgi 19, 20133 Milano, Italy³ and

Department of Physics, National University of Singapore, 117542, Singapore⁴

We present quantum mechanical calculations of autoionization rates for two Rubidium Rydberg atoms with weakly overlapping electron clouds. We neglect exchange effects and consider tensor products of independent atom states forming an approximate basis of the two-electron state space. We consider large sets of two-atom states with randomly chosen quantum numbers and find that the charge overlap between the two Rydberg electrons allows one to characterise the magnitude of the autoionization rates. If the electron clouds overlap by more than one percent, the autoionization rates increase approximately exponentially with the charge overlap. This finding is independent of the energy of the initial state.

PACS numbers: 32.80.Zb, 32.80.Ee, 34.50.-s

I. INTRODUCTION

Exciting ultracold atoms to Rydberg states [1] with large principal quantum number n furnishes the atoms with extremely exaggerated properties. For example, the size, interaction strength and polarizability increases by several orders of magnitude as compared to ground state atoms. This feature allows one to study fundamental physical phenomena on completely new time and length scales and magnifies physical effects such that they become experimentally accessible. For example, dipole-dipole interactions between ground state atoms are typically weak, but they are strong and long-ranged between Rydberg atoms such that μm -sized molecules consisting of two [2–9] and three [10–12] atoms become possible. Moreover, dipole-dipole interactions between Rydberg atoms give rise to the blockade effect [13, 14] and crystals of spatially ordered Rydberg excitations that were experimentally observed in [15]. The modification of the quantum dynamics of Rydberg electrons due to their dipole-dipole interaction has been demonstrated in a recent experiment by Takei *et al.* [16] via ultrafast pump-probe laser techniques.

In systems of dipole-dipole interacting Rydberg atoms the interatomic spacing is typically large compared to the size of the Rydberg electron orbital. A fascinating prospect for future studies is the investigation of Rydberg systems with overlapping electron clouds. In this regime the exaggerated properties of Rydberg atoms would allow one to study the rich physics of electron-electron interactions on much more accessible time and length scales compared to conventional solid state systems. More specifically, the size of the valence electron orbital increases like $R_n = 4n^2 a_0$ where a_0 is the Bohr radius and will thus reach the typical separation between atoms in optical lattices or tweezers for $n \gtrsim 35$. Overlapping electron clouds could give rise to delocalized electrons and correlated quantum many-body states via the strong Coulomb interaction between the electrons. However, these coherent processes compete with autoioniza-

tion and radiative decay processes enabled by the large number of empty orbitals below the Rydberg state.

The first step in investigating the regime of Rydberg atoms with overlapping electron clouds is to characterize the time scales of the occurring physical processes. While radiative processes are well understood [17], we here focus on autoionization of two neutral Rydberg atoms via the Penning effect [1] as shown in Fig. 1. In this process the energy for ionizing atom A is provided by a change in internal energy of atom B. Until now, quantum mechanical calculations of this process are restricted to the dipole-dipole interaction regime of non-overlapping electron clouds [18, 19] where the decay rates are negligibly small. On the contrary, calculations based on classical Hamilton equations [20] show that fast autoionization occurs for atomic separations of the order of R_n where the electron clouds start to overlap. This effect has been identified in [21] as a key factor for understanding the fast autoionization of a Rydberg gas observed in [22]. In order to determine the timescale of autoionization of Rydberg atoms with overlapping electron clouds, quantum mechanical calculations of the corresponding autoionization rates are needed. However, a rigorous approach to this problem is extremely challenging since it would involve finding the highly excited two-electron eigenstates of the system.

In order to estimate autoionization rates of Rydberg atoms with overlapping electron clouds, we here present a simplified model and consider two-atom states $|\psi_M\rangle$ with weakly overlapping electron clouds as shown in Fig. 1. We assume that $|\psi_M\rangle$ is a tensor product of two generally different independent-atom orbitals and neglect exchange effects. In order to account for the fact that these states are not eigenstates of the system, we consider large sets of states $|\psi_M\rangle$ with different quantum numbers that could serve as an approximate basis of the true two-electron eigenstate. We evaluate the autoionization rate of the states $|\psi_M\rangle$ quantum mechanically and show that the charge overlap between the two atoms allows one to characterize the magnitude of the autoionization rates. In the

regime of very small charge overlap between the Rydberg orbitals, the autoionization rates are small and depend on the energy of the initial state. Moreover, the full interaction Hamiltonian can be approximated by its multipole expansion. On the contrary, above a certain threshold the multipole expansion becomes invalid and the autoionization rates increase approximately exponentially with the charge overlap.

Note that the autoionization mechanism between two Rydberg atoms considered here is related to autoionization processes in crystals and clusters that have been termed inter-atomic Auger decay [23] and more recently interatomic Coulombic decay (ICD) [24–27]. In particular, the strong enhancement of autoionization rates through the overlap between electron orbitals in clusters was reported in [25], and ICD processes between several excited atoms in a cluster were studied in [26, 27].

This paper is organized as follows. The system of interest and our model are described in Sec. II. We briefly outline the calculation of the autoionization rates in Sec. III and defer more technical details to Appendix A. In order to account for many different initial states $|\psi_M\rangle$ we randomly select these states as described in Sec. IV. Finally, the autoionization rates of the randomly selected states are presented in Sec. V and a conclusion of our work is given in Sec. VI.

II. THE SYSTEM

We consider two Rydberg atoms as shown in Fig. 1(a), where each atom is comprised of a singly-charged core and one valence electron. We assume that the atoms are so cold that their positions do not change during the decay process. Atom A is centered at the origin and atom B is located at $\mathbf{R} = R\mathbf{e}_z$, where \mathbf{e}_z is the unit vector in z direction and R is the atomic separation. The total Hamiltonian of the two-atom system is $H = H_0 + V$, where $H_0 = H_0^{(A)} + H_0^{(B)}$ and $H_0^{(X)}$ is the Hamiltonian of Rydberg atom X . All interactions between atom A and atom B are described by

$$V = \frac{q^2}{4\pi\epsilon_0} \left(\frac{1}{R} + \frac{1}{|\hat{\mathbf{r}}_1 - \hat{\mathbf{r}}_2|} - \frac{1}{|\hat{\mathbf{r}}_2|} - \frac{1}{|\mathbf{R} - \hat{\mathbf{r}}_1|} \right), \quad (1)$$

where q is the elementary charge and $\hat{\mathbf{r}}_i$ the operator associated with the position of electron i . The first term in Eq. (1) accounts for the repulsion of the two ion cores, the second is the electron-electron interaction and the third (fourth) term describes the interaction of electron 2 (1) with ion core A (B). The eigenstates of H_0 are

$$|\Psi_M\rangle = |\psi_A, \psi_B\rangle, \quad (2)$$

where $|\psi_A\rangle$ and $|\psi_B\rangle$ are independent-atom Rydberg wavefunctions centered at the origin and \mathbf{R} , respectively,

$$\psi_A(\mathbf{r}_1) = \psi_{n_A l_A m_A}(\mathbf{r}_1), \quad \psi_B(\mathbf{r}_2) = \psi_{n_B l_B m_B}(\mathbf{r}_2 - \mathbf{R}). \quad (3)$$

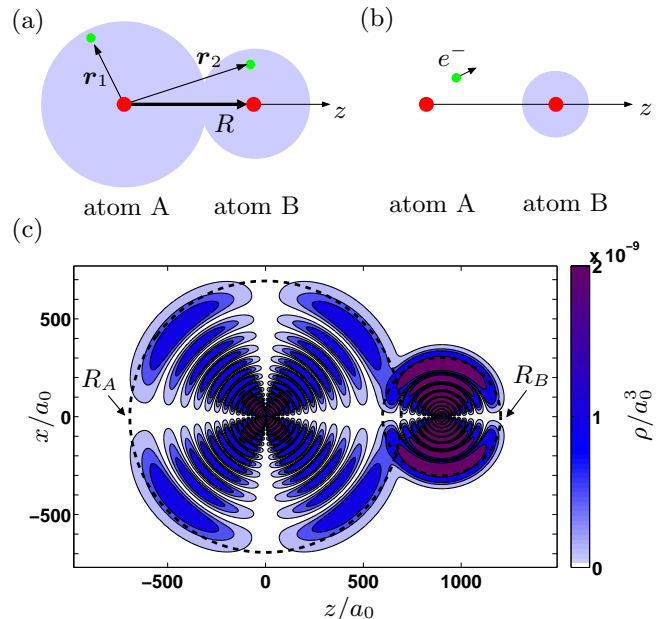


FIG. 1. (Color online) (a) Two Rydberg atoms in different electronic states and with spatial separation R . The blue spheres indicate the size of the Rydberg electron charge density cloud, and \mathbf{r}_i are the electron coordinates. (b) Schematic illustration of the autoionization process. Atom 2 makes a transition into a lower bound state and the electron of atom 1 is ejected into the continuum. (c) Charge density ρ for wave function Ψ_M in Eq. (2) with $n_A = 20$, $l_A = 2$, $m_A = -1$ and $n_B = 15$, $l_B = 1$, $m_B = 1$. The dashed sphere with radius R_A (R_B) denotes the classical outer turning point of the electron of atom A (B).

We ignore the fine structure such that the wavefunctions $\psi_{nlm}(\mathbf{r})$ are characterised by the principal quantum number n , the orbital angular momentum quantum number l and the azimuthal quantum number m . We generate the functions ψ_{nlm} with energy $E_{nl} = -1/[n - \delta_n(l)]^2$ via the Numerov method, where $\delta_n(l)$ is the quantum defect [1, 28]. We choose Rubidium 85 atoms which are a popular choice in recent Rydberg experiments and obtain the energies E_{nl} (and hence the quantum defects) for $n \leq 11$ from spectroscopic data reported in [29]. For $n = 11$, the non-zero quantum defects are $\delta_{11}(0) = 3.134$, $\delta_{11}(1) = 2.652$ and $\delta_{11}(2) = 1.341$ which is consistent with the quantum defects provided in [30]. We ignore the weak dependence of $\delta_n(l)$ on the principal quantum number for $n > 11$. Note that we order the quantum numbers in $|\psi_M\rangle$ such that $E_{n_A l_A} \geq E_{n_B l_B}$ by convention since the state obtained by interchanging A and B has the same autoionization rate.

An example for $|\psi_M\rangle$ is shown in Fig. 1(c), where the size of the electron cloud of atom A (B) is indicated by a sphere of radius R_A (R_B), where R_A (R_B) is the classical outer turning point,

$$R_X = n_X^{*2} + n_X^* \sqrt{n_X^{*2} - l_X(l_X + 1)}, \quad (4)$$

$n^* = [n - \delta_n(l)]$ is the effective quantum number and $X \in \{A, B\}$. In order to quantify the overlap between the wavefunctions $|\psi_A\rangle$ and $|\psi_B\rangle$, we consider the amount of charge due to $|\psi_A\rangle$ inside the sphere V_B with radius R_B around atom B ,

$$\delta q_A(V_B) = q \int_{V_B} |\psi_A|^2 d^3r. \quad (5)$$

Similarly,

$$\delta q_B(V_A) = q \int_{V_A} |\psi_B|^2 d^3r \quad (6)$$

is the amount of charge due to $|\psi_B\rangle$ inside the sphere V_A with radius R_A around atom A . A measure for the differential overlap between $|\psi_A\rangle$ and $|\psi_B\rangle$ is then given by $\delta q/Q$, where $Q = 2q$ is the total electron charge and

$$\delta q = \delta q_A(V_B) + \delta q_B(V_A). \quad (7)$$

In the following we will consider only states with small overlap such that $\delta q/Q \ll 1$.

Note that the physical wavefunction of the two-electron system should include spin degrees of freedom and be completely antisymmetric with respect to electron exchange. However, we find that the simplified state in Eq. (2) results in a good approximation of the autoionization rate for weakly overlapping electron clouds as explained in Sec. III.

III. AUTOIONIZATION RATES

Next we outline the calculation of the autoionization rate for state $|\psi_M\rangle$ in Eq. (2). To this end, we consider the process shown in Fig. 1(b) where atom B makes a transition to a lower bound state $\psi_b(\mathbf{r}_2) \equiv \psi_{n_b l_b m_b}(\mathbf{r} - \mathbf{R})$ with energy $E_b \equiv E_{n_b l_b m_b}$, and the other electron is ejected into the continuum. We model the wavefunction of the ejected electron with mass m_e by energy-normalized Coulomb waves $|\psi_{lm}^E\rangle$ [31, 32] with angular momentum l , magnetic quantum number m and energy E obeying the generalized normalization relation

$$\langle \psi_{lm}^E | \psi_{l'm'}^{E'} \rangle = \delta(E - E') \delta_{ll'} \delta_{mm'}. \quad (8)$$

The Coulomb waves are numerically generated by following the procedure described in [1]. We calculate the autoionization rate using Fermi's golden rule [33] and to first order in the interaction V . The decay rate Γ_M^b for the process shown in Fig. 1(b) is thus given by

$$\Gamma_M^b = \frac{2\pi}{\hbar} \sum_{l_k=0}^{\infty} \sum_{m_k=-l_k}^{l_k} |\langle \psi_{l_k m_k}^{E_k}, \psi_b | V | \psi_M \rangle|^2, \quad (9)$$

where the energy $E_k = E_M - E_b$ of the Coulomb wave is fixed by energy conservation between the initial and final states and

$$E_M = \langle \psi_M | H | \psi_M \rangle \quad (10)$$

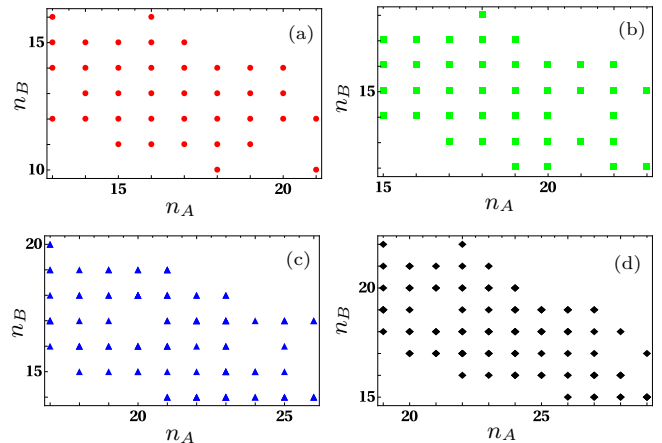


FIG. 2. (Color online) Distribution of the principal quantum numbers n_A and n_B in the randomly chosen sets of states \mathcal{S}_i . (a) Red dots correspond to set \mathcal{S}_1 . (b) Green squares show set \mathcal{S}_2 . (c) Blue triangles are for set \mathcal{S}_3 . (d) Black diamonds correspond to set \mathcal{S}_4 .

is the expectation value of the total Hamiltonian H in the initial state $|\psi_M\rangle$. Note that E_M differs by at most 2% from the unperturbed value $\langle \psi_M | H_0 | \psi_M \rangle = E_{n_A l_A} + E_{n_B l_B}$ for all states considered in Sec. IV. This is consistent with the wavefunctions comprising the initial state being only weakly perturbed by the electron-electron interaction in the overlap region.

A more rigorous calculation with a fully antisymmetric initial state would result in two Coulomb matrix elements in Eq. (9) that are termed the direct and the exchange term [34]. The single matrix element in Eq. (9) corresponds to the direct term, and the exchange term is absent since our initial state $|\psi_M\rangle$ in Eq. (2) is a simple product state. The exchange term depends on the overlap between the single-electron orbitals and decreases exponentially with increasing distance R [25]. Since we are considering only weakly overlapping electron clouds we expect that exchange effects are small and hence the expression in Eq. (9) should be a good approximation for the autoionization rate.

The decay rate Γ_M^b in Eq. (9) accounts for all processes where atom B makes a transition into the bound state $|\psi_b\rangle$ and atom A is ionized. In addition, we consider also the autoionization process with rate $\tilde{\Gamma}_M^b$ where atom A makes a transition to $|\psi_b\rangle$ and atom B is ionized. The full decay rate is then obtained by adding Γ_M^b and $\tilde{\Gamma}_M^b$ and summing over all bound states,

$$\Gamma_M = \sum_{\substack{b \text{ with} \\ E_b \leq E_M}} (\Gamma_M^b + \tilde{\Gamma}_M^b). \quad (11)$$

We numerically evaluate Eq. (11) by restricting the sum over bound states to those with $n_b \geq 0.2(n_A + n_B)$. This is justified since the contribution of lower-lying bound states is negligible. The evaluation of the matrix element in Eq. (11) is described in detail in Appendix A.

In short, we expand all involved wavefunctions and the interaction Hamiltonian V in Eq. (1) in terms of spherical harmonics and limit the integration region to the volume where $|\psi_{A,B}\rangle$ both take on non-negligible values. We restrict the maximum angular momentum in the expansion of the wavefunctions to $l = 1000$, and all terms in the expansion of V leading to an exchange of angular momentum $\Delta l > 15$ between the electrons due to the Coulomb interaction are neglected. With these choices the numerical expense of calculating one value of Γ_M still takes up to 20 hours on a 16 core Intel E5-2640v3 compute node. We estimate that the numerical uncertainty in Γ_M due to these approximations is approximately 10% for initial states with $\delta q/Q > 10^{-4}$, while we achieve full convergence for states with $\delta q/Q \leq 10^{-4}$.

IV. SELECTION OF RANDOM STATES

The two-atom states in Eq. (2) are independent-atom states and thus not eigenstates of the total Hamiltonian H . For sufficiently small atomic separations R , the interaction V couples many states $|\psi_M\rangle$ with different quantum numbers [4, 35]. Here we are not interested in the quantum dynamics of a particular initial state, but the aim is to characterize the autoionization rates of a large variety of different states $|\psi_M\rangle$. To this end, we calculate the autoionization rate Γ_M for four sets \mathcal{S}_i of randomly chosen states that we select as follows. We consider four non-overlapping energy intervals that are centered around the energies $\mathcal{E}_1, \mathcal{E}_2, \mathcal{E}_3$ and \mathcal{E}_4 of the $ndnd$ states with $n = 14, 16, 18$ and 20 , respectively. We then find all two-atom manifolds $n_A l_A n_B l_B$ with $E_{n_A l_A} \geq E_{n_B l_B}$ and within an energy interval of $\pm 5\%$ around \mathcal{E}_i and denote this set of manifolds by \mathcal{M}_i . We only retain those manifolds in \mathcal{M}_i with orbital angular momentum $l_A, l_B \leq 4$. For each set of manifolds \mathcal{M}_i we choose one atomic separation R_i such that most quantum numbers within \mathcal{M}_i give rise to outer turning points R_A and R_B with

$$0.8 \leq \frac{R_i}{R_A + R_B} \leq 1.4. \quad (12)$$

We find that this regime of weakly overlapping electron clouds can be adjusted by choosing $R_1 = 700a_0$, $R_2 = 900a_0$, $R_3 = 1200a_0$ and $R_4 = 1500a_0$, and all manifolds within \mathcal{M}_i that do not obey Eq. (12) are disregarded. After this pre-selection process each set \mathcal{M}_i typically contains several hundred manifolds, and we randomly select 100 manifolds in \mathcal{M}_i that form the set \mathcal{S}_i . Since the total magnetic quantum number is conserved by the interaction Hamiltonian V , we confine our analysis to the $M = 0$ subspace and assign each $n_A l_A$ manifold in \mathcal{S}_i a random magnetic quantum number m_A with $m_B = -m_A$. The distribution of the chosen states with respect to the principal quantum numbers n_A and n_B is shown in Fig. 2 for all four sets. It follows that each set contains a broad distribution of principal quantum

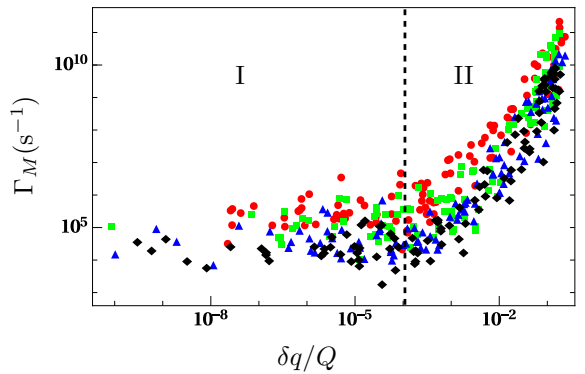


FIG. 3. (Color online) Log-log plot of the autoionization rates Γ_M of the randomly chosen states \mathcal{S}_i as a function of $\delta q/Q$. Red dots correspond to \mathcal{S}_1 , green squares show \mathcal{S}_2 , blue triangles are for \mathcal{S}_3 and black diamonds correspond to \mathcal{S}_4 . The dashed line at $\delta q/Q = 10^{-4}$ separates regions I and II where the autoionization rates behave qualitatively different as a function of the overlap.

numbers where the variation in both n_A and n_B is larger than five.

V. RESULTS AND DISCUSSION

The results for the autoionization rate Γ_M of the randomly chosen states in all sets \mathcal{S}_i are shown in Fig. 3 as a function of the overlap $\delta q/Q$, see Eq. (7). There are two qualitatively different regions I and II divided by the dashed line at $\delta q/Q = 10^{-4}$. In region I the decay rates appear to be independent of the overlap. On the contrary, the decay rates increase sharply with $\delta q/Q$ in region II. In order to understand the physical reason for these two regions we perform reference calculations where we replace the interaction Hamiltonian V in Eq. (1) by its multipole expansion V_{ME} [36] including dipole-dipole, dipole-quadrupole and quadrupole-quadrupole interactions. We find that the autoionization rates calculated with V_{ME} differ by at most 10% from the values obtained with V for all states with $\delta q/Q \leq 10^{-4}$. We thus conclude that the multipole expansion of the interaction Hamiltonian holds if the overlap between the Rydberg orbitals is less than 10^{-4} . On the other hand, the results obtained by V_{ME} and V differ greatly in region II. While all autoionization rates obtained by V_{ME} are smaller than $3 \times 10^7 \text{ s}^{-1}$, those calculated with V can be several orders of magnitude larger for $\delta q/Q \geq 10^{-2}$. This dramatic increase in the autoionization rates with the overlap is consistent with the findings in [25]. It can be explained physically by noting that the full interaction Hamiltonian V allows for direct electron-electron interactions in the region where the charge densities overlap, whereas the leading term in V_{ME} is the dipole-dipole interaction.

In the following we analyse the autoionization rates in regions I and II in more detail. First, we focus on region

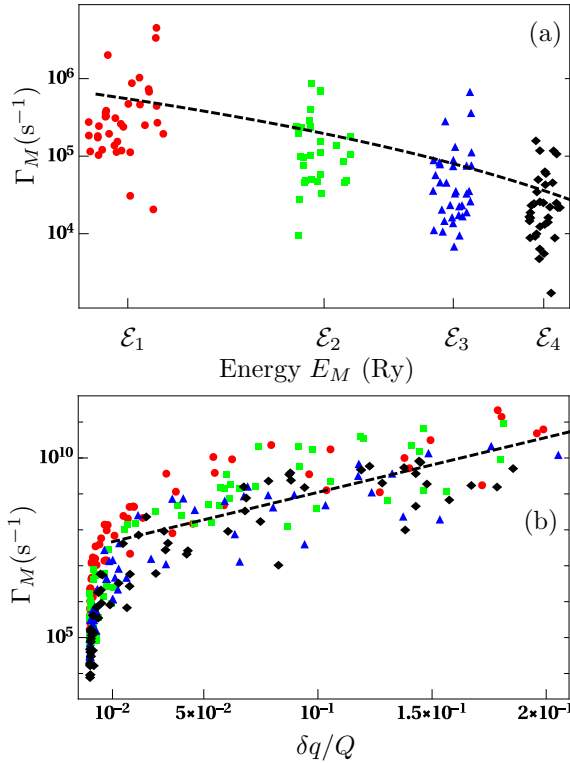


FIG. 4. (Color online) (a) Log-linear plot of the autoionization rates Γ_M of the randomly chosen states \mathcal{S}_i in region I as a function of energy E_M of the initial state. \mathcal{E}_i is the central energy of the interval corresponding to set \mathcal{S}_i (see Sec. IV), and Ry is the Rydberg constant. The dashed line interpolates the four mean decay rates $\langle \Gamma_M \rangle_i$ [see Eq. (13)]. (b) Log-linear plot of the autoionization rates Γ_M of the randomly chosen states \mathcal{S}_i in region II as a function of $\delta q/Q$. The dashed line is an exponential fit to the decay rates Γ_M in all data sets \mathcal{S}_i with $\delta q/Q \geq 10^{-2}$ [see Eq. (14)]. In (a) and (b), red dots correspond to \mathcal{S}_1 , green squares show \mathcal{S}_2 , blue triangles are for \mathcal{S}_3 and black diamonds correspond to \mathcal{S}_4 .

I and plot all autoionization rates Γ_M with $\delta q/Q \leq 10^{-4}$ as a function of the energy E_M of the initial state $|\psi_M\rangle$ as shown in Fig. 4(a). Within each set \mathcal{S}_i , the autoionization rates show no evident energy dependence. The spread in Γ_M is roughly the same for each set \mathcal{S}_i and spans about two orders of magnitude. However, the lower and upper bounds of each set \mathcal{S}_i depend on energy such that the mean decay rates $\langle \Gamma_M \rangle_i$ become gradually smaller by moving from set \mathcal{S}_1 to \mathcal{S}_4 , where $\langle \Gamma_M \rangle_i$ is obtained by averaging over all decay rates Γ_M in \mathcal{S}_i with $\delta q/Q \leq 10^{-4}$. This is illustrated by the dashed line in Fig. 4(a) interpolating the four mean decay rates $\langle \Gamma_M \rangle_i$,

$$\langle \Gamma_M \rangle = \kappa (|E_M|/\text{Ry})^\gamma, \quad (13)$$

where $\kappa = 2.51 \times 10^{12} \text{s}^{-1}$, $\gamma = 3.52$ and Ry is the Rydberg constant. The dominant contribution to the autoionization rate in the multipole regime is the dipole-dipole interaction term such that $\Gamma_M^b \propto d_b^2 d_c^2 R^{-6}$ [19], where d_b is

the dipole matrix element between $|\psi_B\rangle$ and $|\psi_b\rangle$, and d_c is the dipole matrix element between $|\psi_A\rangle$ and a Coulomb wave. The average principal quantum number \bar{n} of the involved Rydberg states increases from set \mathcal{S}_1 to set \mathcal{S}_4 , and hence we expect the involved dipole matrix elements to increase on average with \bar{n}^2 [37]. However, all states in a given set \mathcal{S}_i are evaluated at a given atomic separation R_i [see Sec. IV] with $R_i \approx R_A + R_B \propto \bar{n}^2$ [see Eq. (12)]. It follows that $\Gamma_M^b \propto \bar{n}^{-4}$, and hence we expect the full autoionization rate to decrease with increasing energy of the two-atom state. On the other hand, the large spread in Γ_M within each set \mathcal{S}_i can be explained with the strong dependence of the transition dipole matrix elements on the quantum numbers of the initial and bound states.

Second, we analyze the steep increase of Γ_M in region II. A log-linear plot of the autoionization rates Γ_M in region II is shown in Fig. 4(b) as a function of $\delta q/Q$. We find that Γ_M increases approximately exponentially for $\delta q/Q \geq 10^{-2}$. This is illustrated by the dashed line in Fig. 4(b) given by

$$\Gamma_M = \Gamma_0 10^{\alpha x}, \quad (14)$$

where the parameters $\Gamma_0 = 3.31 \times 10^7 \text{s}^{-1}$ and $\alpha = 15.28$ are obtained by fitting the data points from all sets \mathcal{S}_i with $\delta q/Q \geq 10^{-2}$ to Eq. (14). The spread of the decay rates around the dashed line is roughly three orders of magnitude for $\delta q/Q \leq 0.15$, and reduces to two orders of magnitude for $\delta q/Q > 0.15$. In particular, the autoionization rates are apparently independent of the energy of the initial state if the overlap exceeds several percent.

Finally, we note that the overlap of a given state $|\psi_M\rangle$ is correlated with the symmetry of the energy distribution between the two atoms. More specifically, we consider the symmetry parameter

$$S = 2 \frac{E_{n_A l_A}}{E_M}, \quad (15)$$

where $E_{n_A l_A}$ is the independent-atom energy of state $|\psi_A\rangle$ and E_M is defined in Eq. (10). A value of $S = 1$ corresponds to a completely symmetric distribution of energy E_M between atoms A and B, and S decreases monotonically with reduced symmetry. Figure 5 shows a log-linear plot of S for all sets of states \mathcal{S}_i as a function of $\delta q/Q$, demonstrating that symmetry and overlap are clearly correlated. This result is relevant for systems similar to the experimental setup reported in [22], where a gas of cold atoms was excited to $ndnd$ states by short laser pulses. This initial state is perfectly symmetric with $S = 1$. However, the interatomic distance of some of the atom pairs in the gas will be so small that the dipole-dipole interaction couples the initial state to near-resonant two-atom states with $S < 1$. It follows that even if the autoionization rate of the initial $ndnd$ state is small for atomic pairs with $\delta q/Q < 10^{-4}$, some of the two-atom states involved in the dipole-dipole cascades may autoionize much faster because they have $S < 1$ and hence their overlap can be significantly larger than

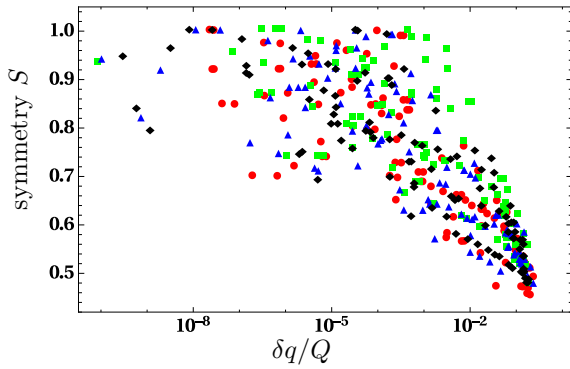


FIG. 5. (Color online) Log-linear plot of the symmetry S [see Eq. (15)] of the randomly chosen states \mathcal{S}_i as a function of $\delta q/Q$. Red dots correspond to \mathcal{S}_1 , green squares show \mathcal{S}_2 , blue triangles are for \mathcal{S}_3 and black diamonds correspond to \mathcal{S}_4 .

for the initial state. A more quantitative analysis of this point can be achieved by a simulation of the full quantum dynamics starting from an experimentally achievable initial state and including all coherent couplings between two-atom states and their autoionization rates. Such an investigation would be an interesting prospect for future studies.

VI. CONCLUSION

In this paper we present quantum mechanical calculations for autoionization rates of two nearby Rydberg atoms. We consider sets of randomly chosen two-atom states and calculate the autoionization rates in lowest order perturbation theory. Since the electron clouds overlap only slightly, we neglect exchange corrections to the autoionization rate. We find that the autoionization rates can be classified via the charge overlap between the two states. If the overlap is less than 10^{-4} , the multipole expansion of the interaction Hamiltonian holds and the autoionization rates are relatively small. In particular, they decrease on average with increasing energy of the two-atom state and can be smaller or comparable to dipole transition rates between near-resonant two-atom states. It follows that the quantum dynamics in this regime will exhibit a rich interplay between coherent transitions and autoionization. However, we find that the autoionization rates increase dramatically beyond the dipole-dipole regime where overlap effects become significant. Our results show that this regime begins where the overlap exceeds 10^{-4} , and an approximately exponential increase sets in if the overlap is larger than 1%. Our calculations were carried out for the specific example of Rubidium atoms. However, our classification of the autoionization rates in terms of the charge overlap makes no reference to the quantum numbers of the initial states or specific properties of Rubidium atoms. We thus expect that our

findings hold for other alkali-metal atoms as well. While we had to restrict our calculations to relatively small principal quantum numbers due to technical reasons, we anticipate that qualitatively similar results should hold for higher principal quantum numbers as well. Extending our current calculations to this regime is subject to further investigation. Other possible extensions of our work include the calculation of the correct two-electron eigenstates via full configuration interaction methods [49], and the application of the complex rotation method [50] in order to find the energies and widths of the two-electron resonances.

In summary, Rydberg atoms with slightly overlapping electron clouds offer fascinating possibilities for future theoretical and experimental studies at the boundary between ultracold atom and molecular physics. In particular, ultrafast pump-probe laser techniques [16] allow one to resolve processes that are much faster than the autoionization rate even if the electron clouds overlap by a few percent. In this way autoionization and coherent processes in correlated Rydberg electron clouds could be measured with unprecedented temporal and spatial resolution. Such experiments would represent a paradigm shift from mimicking electron-electron interactions with ultracold atoms [38–43] to actually realizing them.

ACKNOWLEDGMENTS

We thank the National Research Foundation and the Ministry of Education of Singapore for support. The authors would like to acknowledge the use of the University of Oxford Advanced Research Computing (ARC) facility in carrying out this work (<http://dx.doi.org/10.5281/zenodo.22558>). The research leading to these results has received funding from the European Research Council under the European Unions Seventh Framework Programme (FP7/2007-2013)/ERC Grant Agreement no. 319286 Q-MAC.

Appendix A: Evaluation of the Coulomb matrix element

Here we outline the evaluation of the matrix element

$$M = \langle \psi_{l_k m_k}^{E_k}, \psi_b | V | \psi_A, \psi_B \rangle \quad (\text{A1})$$

entering the autoionization rate in Eq. (9). The operator V in Eq. (1) is a sum of Coulomb interactions $1/|\mathbf{r} - \mathbf{r}'|$ which we expand as

$$\frac{1}{|\mathbf{r} - \mathbf{r}'|} = \sum_{l=0}^{\infty} \sum_{m=-l}^l \frac{4\pi}{2l+1} \frac{r_{<}^l}{r_{>}^{l+1}} Y_l^{m*}(\theta', \phi') Y_l^m(\theta, \phi), \quad (\text{A2})$$

where $r_{<} = \min(r, r')$ and $r_{>} = \max(r, r')$. We truncate the sum over angular momenta l in Eq. (A2) and omit all

terms with $l > 15$. Here l corresponds to Δl in the main text and determines the amount of angular momentum that the Coulomb interaction can transfer between the electrons. In order to evaluate the matrix element M we expand all wavefunctions in terms of spherical harmonics [44]. Since we place atom A at the origin, the expansion of $|\psi_A\rangle$ and $|\psi_{lm}^E\rangle$ comprise only a single term,

$$\psi_A(\mathbf{r}) = R_{n_A l_A}(r) Y_{l_A}^{m_A}(\theta, \phi), \quad (\text{A3a})$$

$$\psi_{lm}^E(\mathbf{r}) = C_{El}(r) Y_l^m(\theta, \phi). \quad (\text{A3b})$$

The wavefunctions $\psi_B(\mathbf{r})$ and $\psi_b(\mathbf{r})$ in Eq. (A1) are centered at atom B . They are both of the form

$$\psi_\beta(\mathbf{r}) = \psi_{n_\beta l_\beta m_\beta}(\mathbf{r} - \mathbf{R}) \quad (\text{A4})$$

with $\psi_{n_\beta l_\beta m_\beta}(\mathbf{r}) = R_{n_\beta l_\beta}(r) Y_{l_\beta}^{m_\beta}(\theta, \phi)$ and $\beta \in \{b, B\}$. Since \mathbf{R} is different from zero we make a general ansatz for the expansion of $\psi_\beta(\mathbf{r})$ in terms of spherical harmonics,

$$\psi_\beta(r, \theta, \phi) = \sum_{l_q=0}^{L_{\max}} \sum_{m_q=-l_q}^{l_q} Q_{l_q}^{m_q}(r) Y_{l_q}^{m_q}(\theta, \phi), \quad (\text{A5})$$

where we expressed \mathbf{r} in terms of spherical coordinates $\mathbf{r}(r, \theta, \phi)$. We set $L_{\max} = 1000$, and the function $Q_{l_q}^{m_q}(r)$

can be found using the orthonormality of $Y_{l_q}^{m_q}$,

$$Q_{l_q}^{m_q}(r) = \int d\theta d\phi \sin \theta \psi_\beta(r, \theta, \phi) Y_{l_q}^{m_q*}(\theta, \phi). \quad (\text{A6})$$

We represent all radial functions on a grid with up to 14000 points. The integration region in Eq. (A6) is restricted to the solid angle where $\psi_\beta(\mathbf{r})$ takes on non-negligible values, and the integral is carried out using the trapezoidal rule [45]. With the expansions in Eqs. (A2), (A3) and (A5) the evaluation of the matrix element M can be reduced to a double integral over the radial variables and the remaining integrals reduce to Gaunt coefficients [46]. The radial integrals are evaluated with the trapezoidal rule [45], and the Gaunt coefficients are defined as

$$\begin{aligned} G_{l_1 l_2 l_3}^{m_1 m_2 m_3} &= \int d\theta d\phi \sin \theta Y_{l_1}^{m_1}(\theta, \phi) Y_{l_2}^{m_2}(\theta, \phi) Y_{l_3}^{m_3}(\theta, \phi) \\ &= (-1)^{m_3} \sqrt{\frac{(2l_1+1)(2l_2+1)}{4\pi(2l_3+1)}} \\ &\quad \langle l_1, l_2; 0, 0 | l_3, 0 \rangle \langle l_1, l_2; m_1, m_2 | l_3, -m_3 \rangle. \end{aligned} \quad (\text{A7})$$

The evaluation of Clebsch-Gordan coefficients [46] $\langle l_1, l_2; m_1, m_2 | l_3, m_3 \rangle$ involves the calculation of factorials which can be numerically unstable for large values of l_1, l_2 and l_3 if floating point numbers are used. In order to circumvent this problem, we generate a library of all non-zero Gaunt coefficients with $l_1, l_2 \leq 1000$ and $l_3 \leq 15$ with the software packet MATHEMATICA [47]. The calculation of Γ_A is implemented in MATLAB [48].

-
- [1] T. F. Gallagher, *Rydberg Atoms* (Cambridge University Press, Cambridge, 1994)
 - [2] C. Boisseau, I. Simbotin, and R. Cot , Phys. Rev. Lett. **88**, 133004 (2002)
 - [3] A. Schwettmann, J. Crawford, K. R. Overstreet, and J. P. Shaffer, Phys. Rev. A **74**, 020701(R) (2006)
 - [4] A. Schwettmann, K. R. Overstreet, J. Tallant, and J. P. Shaffer, J. Mod. Opt. **54**, 2551 (2007)
 - [5] K. R. Overstreet, A. Schwettmann, J. Tallant, D. Booth, and J. P. Shaffer, Nat. Phys. **5**, 581 (2009)
 - [6] N. Samboy, J. Stanojevic, and R. Cote, Phys. Rev. A **83**, 050501(R) (2011)
 - [7] N. Samboy and R. Cote, J. Phys. B **44**, 184006 (2011)
 - [8] M. Kiffner, H. Park, W. Li, and T. F. Gallagher, Phys. Rev. A **86**, 031401(R) (2012)
 - [9] M. Kiffner, W. Li, and D. Jaksch, Phys. Rev. Lett. **110**, 170402 (2013)
 - [10] N. Samboy and R. C  t , Phys. Rev. A **87**, 032512 (2013)
 - [11] M. Kiffner, W. Li, and D. Jaksch, Phys. Rev. Lett. **111**, 233003 (2013)
 - [12] M. Kiffner, M. Huo, W. Li, and D. Jaksch, Phys. Rev. A **89**, 052717 (2014)
 - [13] E. Urban, T. A. Johnson, T. Henage, L. Isenhower, D. D. Yavuz, T. G. Walker, and M. Saffman, Nat. Phys. **5**, 110 (2009)
 - [14] A. Ga  tan, Y. Miroshnychenko, T. W. an A. Chotia, M. Viteau, D. Comparat, P. Pillet, A. Browaeys, and P. Grangier, Nat. Phys. **5**, 115 (2009)
 - [15] P. Schau , M. Cheneau, M. Endres, T. Fukuhara, S. Hild, A. Omran, T. Pohl, C. Gross, S. Kuhr, and I. Bloch, Nature **491**, 87 (2012)
 - [16] N. Takei and C. Sommer and C. Genes and G. Pupillo and H. Goto and K. Koyasu and H. Chiba and M. Weidem  ller and K. Ohmori, arXiv:1504.03635v1.
 - [17] I. I. Beterov, I. I. Ryabtsev, D. B. Tretyakov, and V. M. Entin, Phys. Rev. A **79**, 052504 (2009)
 - [18] Y. Hahn, J. Phys. B **33**, L655 (2000)
 - [19] T. Amthor, J. Denskat, C. Giese, N. N. Bezuglov, A. Ekers, L. S. Cederbaum, and M. Weidem  ller, Eur. Phys. J. D **53**, 329 (2009)
 - [20] F. Robicheaux, J. Phys. B **38**, S333 (2005)
 - [21] F. Robicheaux, M. M. Goforth, and M. A. Phillips, Phys. Rev. A **90**, 022712 (2014)
 - [22] P. J. Tanner, J. Han, E. S. Shuman, and T. F. Gallagher, Phys. Rev. Lett. **100**, 043002 (2008)
 - [23] J. A. D. Matthew and Y. Komninos, Surf. Sci. **53**, 716 (1975).

- [24] L. S. Cederbaum, J. Zobeley, and F. Tarantelli, Phys. Rev. Lett. **79**, 4778 (1997).
- [25] V. Averbukh, I. B. Müller, and L. S. Cederbaum, Phys. Rev. Lett. **93**, 263002 (2004)
- [26] A. I. Kuleff, K. Gokhberg, S. Kopelke, and L. S. Cederbaum, Phys. Rev. Lett. **105**, 043004 (2010).
- [27] Y. Ovcharenko, V. Lyamayev, R. Katzy, M. Devetta, A. LaForge, P. O’Keeffe, O. Plekan, P. Finetti, M. Di Fraia, M. Mudrich, M. Krikunova, P. Piseri, M. Coreno, N. B. Brauer, T. Mazza, S. Stranges, C. Grazioli, R. Richter, K. C. Prince, M. Drabbels, C. Callegari, F. Stienkemeier, and T. Möller, Phys. Rev. Lett. **112**, 073401 (2014).
- [28] M. L. Zimmerman, M. G. Littman, M. M. Kash, and D. Kleppner, Phys. Rev. A **20**, 2251 (1979)
- [29] F. Luna, G. H. Cavalcanti, L. Coutinho, and A. G. Trigueiros, J. Quant. Spectrosc. Radiat. Transfer **75**, 559 (2002)
- [30] W. Li, I. Mourachko, M. W. Noel, and T. F. Gallagher, Phys. Rev. A **67**, 052502 (2003).
- [31] H. Friedrich, *Theoretical Atomic Physics* (Springer, Berlin, 2006)
- [32] W. P. Spencer, A. G. Vaidyanathan, D. Kleppner, and T. W. Ducas, Phys. Rev. A **26**, 1490 (1982)
- [33] C. Cohen-Tannoudji, J. Dupont-Roc, and G. Grynberg, *Atom-Photon Interactions* (1998)
- [34] P. J. Feibelman, E. J. McGuire, and K. C. Pandey, Phys. Rev. B **15**, 2202 (1977)
- [35] J. S. Cabral, J. M. Kondo, L. F. Goncalves, V. A. Nascimento, L. G. Marcassa, D. Booth, J. Tallant, A. Schwettmann, K. R. Overstreet, J. Sedlacek, and J. P. Shaffer, J. Phys. B **44**, 184007 (2011)
- [36] M. R. Flannery, D. Vrinceanu, and V. N. Ostrovsky, J. Phys. B **38**, S279 (2005)
- [37] T. G. Walker and M. Saffman, Phys. Rev. A **77**, 032723 (2008)
- [38] R. Jördens, N. Strohmaier, K. Gnter, H. Moritz, and T. Esslinger, Nature **455**, 204 (2012)
- [39] R. N. Palmer and D. Jaksch, Phys. Rev. Lett. **96**, 180407 (2006)
- [40] N. R. Cooper and J. Dalibard, Phys. Rev. Lett. **110**, 185301 (2013)
- [41] I. Bloch, J. Dalibard, and W. Zwerger, Rev. Mod. Phys. **80**, 885 (2008)
- [42] J. Simon, W. S. Bakr, R. Ma, M. E. Tai, P. M. Preiss, and M. Greiner, Nature **472**, 307 (2011)
- [43] C. Sanner, E. J. Su, W. Huang, A. Keshet, J. Gillen, and W. Ketterle, Phys. Rev. Lett. **108**, 240404 (2012)
- [44] C. Cohen-Tannoudji, B. Diu, and F. Laloë, *Quantum Mechanics (Volume I)* (London, 1977)
- [45] M. Abramowitz and I. A. Stegun (Eds.), *Handbook of Mathematical Functions with Formulas, Graphs, and Mathematical Tables, 9th printing.* (Dover, New York, 1972)
- [46] C. Cohen-Tannoudji, B. Diu, and F. Laloë, *Quantum Mechanics (Volume II)* (London, 1977)
- [47] Wolfram Research, Inc., *Mathematica Version 10.1* (Wolfram Research, Inc., Irvine, Champaign, Illinois)
- [48] MATLAB, *version 8.4.0 (R2014b)* (The MathWorks Inc., Natick, Massachusetts, 2014)
- [49] J. Olsen, B. O. Roos, P. Jørgensen, and H. J. A. Jensen, J. Chem. Phys. **89**, 2185 (1988).
- [50] Y. K. Ho, Phys. Rep. **99**, 1 (1983).